JCI The Journal of Clinical Investigation

Glucocorticoid receptor dimers control intestinal STAT1 and TNF-induced inflammation in mice

Marlies Ballegeer, … , Roosmarijn E. Vandenbroucke, Claude Libert

J Clin Invest. 2018. https://doi.org/10.1172/JCI96636.

Research Article In-Press Preview **Endocrinology** **Immunology**

Graphical abstract

Find the latest version:

https://jci.me/96636/pdf

Glucocorticoid receptor dimers control intestinal STAT1 and TNF-induced inflammation in mice

Marlies Ballegeer[1,2], Kelly Van Looveren[1,2], Steven Timmermans[1,2], Melanie Eggermont[1,2], Sofie Vandevyver[1,2], Fabien Thery[3,4], Karen Dendoncker[1,2], Jolien Souffriau[1,2], Jolien Vandewalle[1,2], Lise Van Wyngene[1,2], Riet De Rycke[1,2], Nozomi Takahashi[1,2], Peter Vandenabeele[1,2], Jan Tuckermann[5], Holger M. Reichardt[6], Francis Impens[3,4,7], Rudi Beyaert[1,2], Karolien De Bosscher[4,8], Roosmarijn E. Vandenbroucke[1,2] and Claude Libert[1,2]

[1] Inflammation Research Center, VIB, Ghent, Belgium
[2] Department of Biomedical Molecular Biology, Ghent University, Ghent, Belgium
[3] VIB-UGent Center for Medical Biotechnology, VIB, B-9000 Ghent, Belgium
[4]Department of Biochemistry, Ghent University, B-9000 Ghent, Belgium
[5] Institute of Comparative Molecular Endocrinology, University of Ulm, Ulm, Germany
[6] Institute for Cellular and Molecular Immunology, University of Göttingen Medical School, Göttingen, Germany
[7] VIB Proteomics Core, VIB, B-9000 Ghent, Belgium
[8] Receptor Research Laboratories, Nuclear Receptor Lab, Medical Biotechnology Center, VIB, Ghent, Belgium

Marlies Ballegeer and Kelly Van Looveren share first authorship

Corresponding author

Claude Libert
Inflammation Research Center
Technologiepark, 927
9052 Ghent
Belgium
Phone: +32 9 3313700
Claude.Libert@IRC.VIB-UGent.be

Abstract

Tumor Necrosis Factor (TNF) is an important mediator in numerous inflammatory diseases, e.g. in inflammatory bowel diseases (IBD). In IBD, acute increases in TNF production can lead to disease flares. Glucocorticoids (GCs), which are steroids that bind and activate the glucocorticoid receptor (GR), are able to protect animals and humans against acute TNF-induced inflammatory symptoms. Mice with a poor transcriptional response of GR-dimer-dependent target genes were studied in a model of TNF-induced lethal inflammation. In contrast to the $GR^{wt/wt}$ mice, these $GR^{dim/dim}$ mice displayed a significant increase in TNF sensitivity and a lack of protection by the GC dexamethasone (DEX). Unchallenged $GR^{dim/dim}$ mice had a strong interferon-stimulated gene (ISG) signature, along with STAT1 upregulation and phosphorylation. This ISG signature was gut specific and, based on our studies with antibiotics, depended on the gut microbiota. GR dimers directly bound to short DNA sequences in the STAT1 promoter known as inverted repeat negative GRE (IR-nGRE) elements. Poor control of STAT1 in $GR^{dim/dim}$ mice led to failure to repress ISG genes resulting in excessive necroptosis induction by TNF. Our findings support a critical interplay between gut microbiota, interferons, necroptosis and GR in both the basal response to acute inflammatory challenges and in the pharmacological intervention by GCs.

Introduction

The cytokine Tumor Necrosis Factor (TNF) is of great interest in biomedical research. Low but chronic expression levels of TNF have been shown to be sufficient for the development of diseases which have a big economic and social impact, e.g. rheumatoid arthritis and inflammatory bowel diseases, such as Crohn disease. For the treatment of these, and other diseases, TNF inhibiting biological drugs have been shown to be a good option for patients not responding to first-line treatments for example with methotrexate (1). Although anti-TNF treatment is often successful, there are a number of problems associated with anti-TNF therapy, such as side-effects, non-responsiveness and high cost (1). Interestingly, in such chronic diseases, acute exacerbations leading to inflammation flares are observed which may be caused by several molecules, including damage-associated molecular patterns (DAMPS) and cytokines, including an acute increase in TNF production (2). Therefore, understanding the impact, mechanism and therapeutic inhibition of acute TNF-induced toxicity is essential.

Although there is debate about their underlying mechanism of action, glucocorticoids (GCs) are used in the management of several acute inflammatory conditions. TNF-induced acute lethal inflammation represents an interesting mouse model, in which the intestinal epithelial cells (IECs) have been described to be the main target cells of TNF (3–5). In mice, at least two gut-associated mechanisms contribute to loss of IEC barrier function, which is a crucial step in TNF-induced lethality: (i) loss of mucus in goblet cells and loss of antibacterial granules in Paneth cells, (ii) damage and cell death in the IEC layer (5, 6).

GCs protect against TNF-induced lethal shock and TNF-induced intestinal permeability (5). GCs, such as dexamethasone (DEX), bind and activate the glucocorticoid receptor (GR) (7). They are used to treat a variety of inflammatory disorders such as rheumatoid arthritis and inflammatory bowel diseases (8). After binding, GR moves to the nucleus and regulates gene transcription as a monomer or as a homodimer. For a long time, the anti-inflammatory effects of GCs were believed to

result mainly from tethering (i.e. protein-protein interactions) of monomeric GR to inflammatory transcription factors such as NF-κB and AP-1. However, more recent research indicates that GR homodimers, which form a DNA-binding transcription factor, are essential to mediate the anti-inflammatory properties of GCs in acute inflammatory settings, such as Systemic Inflammatory Response Syndrome (SIRS) (9, 10). Most of these data are based on findings in $GR^{dim/dim}$ mice. These mice express a mutant version of GR, carrying a missense point mutation (A458T) which leads to a reduced GR dimerization and DNA binding, yet maintains an intact monomer profile (11, 12). Upon injection of synthetic GCs, $GR^{dim/dim}$ mice show a significantly reduced expression of glucocorticoid response element (GRE) responsive target genes (9, 13, 14). The $GR^{dim/dim}$ mutant protein binds much less strong to the classical type imperfect palindrome GRE [$AGAACA(N)_3TGTTCT$] (12). As described by Surjit *et al.*, GR dimers additionally downregulate several hundreds of genes, by interaction with a short inverted repeat GRE (IR-nGRE), defined as [$CTCC(N)_{0-2}GGAGA$] (15). $GR^{dim/dim}$ mice are extremely sensitive in mouse models of contact hypersensitivity, endotoxemia and sepsis as well as in the TNF-induced SIRS model (9, 10). Anti-inflammatory pathways induced by GR dimers are hampered in $GR^{dim/dim}$ mice. For example, a crucial role for the GC inducible and GR-dimer-dependent gene *Dusp1,* encoding MKP1, was described in the TNF model and for the *Il1ra* gene, encoding the IL1 receptor antagonist, in the endotoxemia model (9, 10).

Here, we studied the mechanism by which GR dimers control TNF-mediated pathological changes at the level of the IECs. We measured genome wide mRNA expression profiles of PBS-, TNF- and DEX-stimulated IECs of $GR^{wt/wt}$ and $GR^{dim/dim}$ mice. In non-stimulated conditions, we found an IEC-specific interferon-stimulated gene (ISG) signature in $GR^{dim/dim}$ mice, likely driven by STAT1 and strongly reduced by antibiotics treatment. Our data suggest a tight interplay between gut microbiota, induction of ISGs and repression by locally produced GCs and GR dimers. They also explain why $GR^{dim/dim}$ mice are extremely sensitive to SIRS and why exogenous GCs, such as DEX, fail to protect $GR^{dim/dim}$ mice against TNF-induced intestinal permeability and lethality. Among the ISGs, induced by TNF but poorly controlled in $GR^{dim/dim}$ mice, are genes essential in necroptosis. *Ripk3, Zbp1* and *Mlkl*

were identified, suggesting that necroptosis is a process promoted by microbiome and interferons (IFNs) and controlled by dimeric GR. Therefore, we conclude that under physiological conditions, the microbiota sustain a local GC production in order to prevent a detrimental ISG expression signature induced by the very same microbiota in a GR dimer-dependent way. Failure of this protective loop leads to extreme sensitization for cell death in IECs and TNF-induced gut permeability and subsequent lethality.

Results

Intestinal epithelial GR and GR dimers play an essential role in the protection against TNF-induced lethality, gut permeability and cell death

We previously published that $GR^{dim/dim}$ mice display a significant increase in sensitivity towards TNF-induced lethality and that TNF lethality is linked with apparent loss of goblet cells and Paneth cells and permeability of the IECs (5, 9). Hence, we decided to study the role of GR dimers in the intestinal epithelium during TNF-induced SIRS. $GR^{VillinKO}$ mice, which selectively lack a functional GR-coding gene *(Nr3c1)* in intestinal epithelial cells (IECs) were used (16). $GR^{VillinKO}$ and control $GR^{flox/flox}$ mice were injected with a single dose of 35 µg TNF and survival was monitored. $GR^{VillinKO}$ mice were significantly more sensitive compared to the control $GR^{flox/flox}$ mice (**Figure 1A**). It has been known for a long time that injection of GCs protects against TNF-induced lethal shock (7). Interestingly, DEX could not protect $GR^{VillinKO}$ mice (**Figure 1A**), strongly indicating that the protection by DEX requires GR expression in IECs.

To investigate the importance of GR dimers in the protection against TNF lethality by exogenous GCs, we pre-treated $GR^{wt/wt}$ and $GR^{dim/dim}$ mice with 10 mg/kg DEX or PBS, followed by increasing doses of TNF. Survival was monitored (**Figure 1B**) and an LD_{50} was defined for all mouse groups (**Figure 1C**). $GR^{dim/dim}$ mice displayed a higher sensitivity for TNF compared to $GR^{wt/wt}$ mice, with LD_{50} values of respectively 10 µg and 30.5 µg per mouse. In $GR^{wt/wt}$ mice, a single injection of DEX increased the LD_{50} of TNF over three times (from 30.5 µg to 96.8 µg per mouse), but in $GR^{dim/dim}$

mice DEX had no significant protective effect and increased the LD_{50} from 10 µg to 11.9 µg per mouse. Our data suggest an essential role for IEC GR and in particular an optimal dimerization function in resistance against TNF-induced lethal shock, both in absence and presence of exogenous GCs.

Next, we investigated whether GR dimers in IECs protect against TNF by reducing intestinal permeability previously shown to be strongly linked with TNF lethality (5). We studied the intestinal permeability, and cell death of IECs in the ileum of $GR^{wt/wt}$ and $GR^{dim/dim}$ mice after TNF challenge. In both groups of mice we used 12.5 µg of TNF, which is a lethal dose in $GR^{dim/dim}$ mice but not lethal in $GR^{wt/wt}$ mice. In contrast to $GR^{wt/wt}$ mice, $GR^{dim/dim}$ mice displayed significant increased intestinal permeability determined via FITC-dextran leakage into the blood upon oral gavage (**Figure 1D**), and bowel damage as judged by H&E staining after TNF challenge (**Figure 1E**). $GR^{dim/dim}$ mice also displayed TNF-induced cell death of IECs, while this was virtually absent in $GR^{wt/wt}$ mice, as quantified by TUNEL stainings. Positive red signals were particularly prominent at the villi tops and less so in the crypts (**Figure 1F**).

GR dimers are essential to suppress STAT1 expression and activity specifically in the gut

In order to investigate why $GR^{dim/dim}$ mice are sensitive to these TNF-induced effects on IECs, we performed an RNA sequencing (RNAseq) analysis of IECs of $GR^{wt/wt}$ and $GR^{dim/dim}$ mice 8h after injection with PBS or with TNF. In control PBS injected mice, respectively 460 and 240 genes showed significantly up and down regulation in $GR^{dim/dim}$ compared to $GR^{wt/wt}$ IECs (**Supplemental File SF1**). Known motif analysis of the differentially expressed (DE) genes by HOMER revealed a significant enrichment of ISRE, IRF1 and IRF2 motif-containing genes in IECs of $GR^{dim/dim}$ compared to $GR^{wt/wt}$ mice (**Figure 2A**). For example, upregulation of *Ifit1*, *Stat1, Irf8* and *Irf1* in IECs of $GR^{dim/dim}$ mice was found (**Figure 2B**). Additionally, **Supplemental File SF2** displays a more extensive heat map of interferon-stimulated genes (ISGs) and **Supplemental File SF3** lists all ISGs higher and lower expressed in $GR^{dim/dim}$ compared to $GR^{wt/wt}$ IECs. These data were confirmed via qPCR (**Figure 2C**). Out

of 460 genes significantly higher expressed in IECs of $GR^{dim/dim}$ mice, 228 were genes defined as belonging to the "Interferome" database (17), which is a much higher frequency than expected by chance (Hypergeometric test p-value of 1.61×10^{-66}).

The induction of ISGs such as *Ifit1,* is under the control of the transcription factor complex IFN-stimulated gene factor 3 (ISGF3) which consists of STAT1, STAT2 and IRF9 (18). In agreement with the fact that many of the STAT1 responsive ISG genes are up-regulated in $GR^{dim/dim}$ mice -suggesting an active ISGF3 complex-, we found that STAT1 protein levels were increased in $GR^{dim/dim}$ mice compared to $GR^{wt/wt}$ mice and that STAT1 is only phosphorylated in IECs of $GR^{dim/dim}$ mice. (**Figure 2D and 2E**). Furthermore, an ISG signature was detected in the IECs of $GR^{VillinKO}$ mice (**Figure 2F**), suggesting that the ISG signature is mediated by a lack of local (dimeric) GR signaling.

To confirm that the ISG signature in IECs of $GR^{dim/dim}$ mice is also observed at the protein level, we performed a proteome-wide Mass Spectrometry (LC-MS/MS) experiment on ileum samples of $GR^{wt/wt}$ and $GR^{dim/dim}$ mice. Differential protein concentrations with a LFC of 1.0 and an adjusted p-value of 0.05 were listed in **Supplemental File SF4**. We found 32 proteins upregulated in $GR^{dim/dim}$, including 17 known as Interferon-stimulated (18) (17/32 significant enrichment of Interferome proteins p=0.003), including STAT1.

A conceivable interpretation of our data is that GR mediates repression of ISGs via the control of STAT1 expression in a GR dimer-dependent way. To repress gene expression in a GR dimer-dependent way, the gene should contain one or more negative or inhibitory GREs in its promoter. By motif analysis we identified two so-called "IR-nGRE elements" as defined in (15), in the promoter of STAT1: IR-nGRE1 with sequence CACCTGGAGA and IR-nGRE2 with sequence CTCCAGGACA at positions -2841 and -757 relative to the transcription start site, respectively. We studied GR binding to these elements via chromatin immunoprecipitation (ChIP) on ileum tissue extracts (**Figure 2G**). In the graph, data is represented as the fold-change of the GR specific H300 antibody to IgG control thus showing specific recruitment of GR to both IR-nGRE elements in the STAT1 promoter (ratio GR

to IgG control). In basal conditions, GR was recruited to the IR-nGRE elements in the STAT1 promoter in both $GR^{wt/wt}$ mice and $GR^{dim/dim}$ mice as shown by a 2-fold change. Interestingly, GR was significantly more recruited to these elements upon DEX treatment in $GR^{wt/wt}$ mice compared to DEX treated $GR^{dim/dim}$ mice. These data potentially validate the IR-nGRE elements in the STAT1 promoter as GR dimer-bound elements which might be involved in the GR dimer-dependent repression of *Stat1* gene expression.

The IEC-specific ISG signature and corticosterone production in $GR^{dim/dim}$ mice are modulated by the gut microbiome.

Interestingly, the increased expression of *Stat1* mRNA observed in $GR^{dim/dim}$ mice was only observed in intestinal epithelium and not in other organs such as liver, macrophages, spleen and adrenal glands (**Figure 3A**). The gut is an unique organ where local GCs are produced and where the gut microbiota is present (19). Microbiota is known to trigger signaling pathways leading to the production of IFNs and activation of their signaling cascades (20–22). We hypothesize that under basal GR wildtype conditions, IFN signaling in IECs is stimulated by the microbiota, but that this IFN response is controlled by local GC production which leads to low but important GR dimer repressor activity.

To investigate this hypothesis, we studied the effect of the microbiome on the basal gene expression in the IECs of $GR^{wt/wt}$ and $GR^{dim/dim}$ mice. Both groups of mice were treated with an antibiotic cocktail (+AB) for three weeks to deplete the bacteria, which was confirmed by plating out stool samples. In both groups of mice, antibiotics treatment reduced *Stat1* and *Ifit1* expression in IECs (**Figure 3B and 3C**). Following mRNA expression, total STAT1 protein levels were reduced in both groups of mice after antibiotic treatment. In addition, a downward trend in the levels of phosphorylated STAT1 was observed in $GR^{dim/dim}$ mice only ($p=0.07$) as there are no P-STAT1 levels measureable in $GR^{wt/wt}$ mice (**Figure 2D and 2E)**. Interestingly, in $GR^{dim/dim}$ mice the levels of *Stat1* and *Ifit1* mRNA after antibiotic treatment remained higher than in untreated $GR^{wt/wt}$ mice, suggesting that

not only the triggering of TLRs or IFN-β production by the antibiotic-sensitive microbiota induces the ISG signature in the $GR^{dim/dim}$ mice, but that additional factors, such as e.g. antibiotics-resistant bacteria, viruses and fungi, are involved. The reduction in the ISG signature by antibiotics was somewhat reflected in the sensitivity to TNF-induced lethality because antibiotics treated $GR^{wt/wt}$ and $GR^{dim/dim}$ mice were found to be partly protected (**Figure 3D**).

Next to adrenal cortical cells, IECs are known to produce GCs (19). Therefore, local stimulation of corticosterone (CS) production by microbiota components could be an additional factor needed to control the ISG signature in the IECs. To address this, we first studied the impact of antibiotics on the expression of the *Cyp11a1* and *Cyp11b1* genes, which encode critical steroidogenic enzymes involved in CS synthesis, in IECs of $GR^{wt/wt}$ and $GR^{dim/dim}$ mice . In both mouse groups the expression of these genes was reduced in IECs of mice subjected to antibiotics, supporting our hypothesis (**Figure 3E and 3F**). Interestingly, the expression of *Cyp11a1* and *Cyp11b1* genes was higher in $GR^{dim/dim}$ mice compared to $GR^{wt/wt}$ mice. This correlates with the fact that both genes are known ISG genes, and are found in the *Interferome* database (17). Next, the local production of CS in IECs in the absence of microbiota was determined. Interestingly, *ex vivo* CS production by ileum explants was significantly reduced by antibiotics treatment in mice (**Figure 3G**). Serum CS levels, which are higher in $GR^{dim/dim}$ than $GR^{wt/wt}$ mice (23) , were also reduced about half by antibiotics (data not shown). Altogether, these data support our hypothesis that microbiota stimulate local CS production and activate GR dimers, which are essential in controlling the microbiota-stimulated ISG signature in the gut.

STAT1 and its responsive genes are master regulators of sensitivity to TNF

STAT1 deficient ($STAT1^{-/-}$) mice exhibit strong IFN signaling defects and do not display any of the physiological responses associated with IFNs (24–26). In contrast to $STAT1^{+/+}$ mice, full $STAT1^{-/-}$ mice fail to express *Ifit1, Ifit2* or other ISGs (including *Cyp11a1* and *Cyp11b1*) in IECs in unstimulated conditions (**Figure 4A**). $STAT1^{-/-}$ mice were found to resist a lethal dose of TNF (**Figure 4B**), as well as

TNF-induced intestinal permeability or cell death (**Figure 4C and 4D**). These data support the idea that STAT1 is a crucial regulator of TNF-induced intestinal permeability, IEC cell death and subsequent lethality. Unfortunately, homozygous STAT1$^{-/-}$ GR$^{dim/dim}$ double mutant mice were not viable. To investigate if the upregulated and phosphorylated intestinal STAT1 is a master regulator of GR$^{dim/dim}$ hypersensitivity to TNF, we administered the JAK/STAT inhibitor Tofacitinib (27). Tofacitinib (100 mg/kg) or vehicle was given orally to GR$^{dim/dim}$ mice. Mice received Tofacitinib twice a day for 2 days before challenge with 20 μg of TNF and two times (1h before and 8h after) on the day of the challenge. Compared to treatment with vehicle, Tofacitinib treatment significantly protected GR$^{dim/dim}$ mice against TNF-induced lethality (**Figure 4E**).

To further explore how the gut ISGs signature might be connected to the increased sensitivity of GR$^{dim/dim}$ mice to TNF, we studied gene expression profiles in IECs of GR$^{wt/wt}$ and GR$^{dim/dim}$ mice challenged with different doses of TNF. Mice were injected with 12.5 μg of TNF, which is a sublethal dose in GR$^{wt/wt}$ mice (referred to as WT12.5) but is a lethal dose in GR$^{dim/dim}$ mice (DIM12.5). GR$^{wt/wt}$ mice were also challenged with a lethal dose (50 μg) of TNF (WT50). A comparison between the response to different doses of TNF is discussed in **Supplemental File SF5.** Ingenuity Pathway Analysis (IPA) revealed that the major pathway activated by lethal doses of TNF in GR$^{wt/wt}$ and GR$^{dim/dim}$ is the "Interferon Signaling" pathway. When focusing on all 2029 genes which are significantly induced by TNF (across the three groups), 736 of these genes were identified as ISGs by the Interferome database (17). In both GR$^{wt/wt}$ and GR$^{dim/dim}$ mice, a dose of 12.5 μg TNF induces an almost identical set of ISGs, but TNF induction of these genes was significantly higher in GR$^{dim/dim}$ than in GR$^{wt/wt}$ mice (**Figure 4F**, log Y axis). This is also illustrated by the expression pattern of *Ifit1* and *Ifit2* (**Figure 4G**). Together, these results suggest a poorly controllable ISG induction in GR$^{dim/dim}$ mice upon TNF challenge. Based on the data with STAT1 deficient mice (**Figure 4C**) and our previous work using IFN- and IFN-receptor-1 deficient mice (3), the unsufficient control of ISG induction in GR$^{dim/dim}$ mice is likely to form the basis of their hypersensitivity to TNF-induced lethality.

Lack of protective effects of exogenous GCs against TNF-induced changes in the gut of $GR^{dim/dim}$ mice

To study the effect of exogenous GCs on TNF-induced intestinal permeability, we pre-treated mice with vehicle or DEX (-30 min) and challenged $GR^{wt/wt}$ and $GR^{dim/dim}$ mice with a lethal dose of TNF, 50 µg and 12.5 µg respectively. 8h after TNF challenge, the TNF-induced intestinal permeability was significantly decreased by DEX in $GR^{wt/wt}$ mice, but not in $GR^{dim/dim}$ mice (**Figure 5A**). To determine the damage of the intestine, ileum sections were made 2h and 8h after TNF challenge and damage was quantified visually using the validated protocol (28), including scores for villus length, villus erosion, cell death and loss of goblet cells (**Figure 5B**). TNF caused massive damage to the gut in all samples. DEX was able to protect partially against the TNF-induced damage to the villi in $GR^{wt/wt}$ mice but not in $GR^{dim/dim}$ mice. TUNEL staining on ileum sections 8h after TNF challenge revealed more TUNEL activity induced by TNF in $GR^{dim/dim}$ compared to $GR^{wt/wt}$ mice. Moreover, DEX had a significant protective effect in $GR^{wt/wt}$ mice but not in $GR^{dim/dim}$ mice (**Figure 5C**).

GR dimer-specific repression of ISGs including necroptosis master switches *Ripk3*, *Zbp1* and *Mlkl*

To identify the biological pathway behind the observed GR-dimer dependent protective effects in Figure 5A-C, we studied the effects of DEX on gene expression by RNAseq of $GR^{wt/wt}$ and $GR^{dim/dim}$ IECs 8h after TNF or PBS, pre-treated with PBS or DEX (-30 min) (set-up in **Figure 5D**). An overview of the numbers of DE genes (UP and DOWN) in the DEX conditions, relative to non-induced (PBS injected) levels is provided in **Figure 5E**. No specifically enriched motifs were found by HOMER in the $GR^{dim/dim}$-specific regulated genes. As expected, one of the prominent enriched motifs found in the family of $GR^{wt/wt}$-specific DEX-induced genes is the classical GRE. Interestingly, the major motifs found in $GR^{wt/wt}$-specific DEX downregulated genes are ISRE and IRF motifs (**Figure 5F**).

A dimer-specific repression of ISGs seems a plausible mechanism underlying the molecular basis of the GR dimer-specific protection of DEX against TNF-induced gut permeability and lethality. To investigate whether DEX represses TNF-induced ISRE genes more prominently in $GR^{wt/wt}$ compared

to $GR^{dim/dim}$ mice, we studied *Stat1* and *Ifit1* gene expression profiles in both mice groups (**Figure 6A and 6B)**. Although DEX is able to repress TNF-induced expression of these genes, the process is less efficient in $GR^{dim/dim}$ mice compared to $GR^{wt/wt}$ mice. As mentioned before, we found DEX-stimulated GR recruitment to both IR-nGRE elements found in the STAT1 promoter upon DEX treatment, but only in $GR^{wt/wt}$ mice (Figure 2G). When evaluating the impact of DEX on transcriptional levels of TNF-induced ISGs specifically in $GR^{wt/wt}$ and $GR^{dim/dim}$ mice, we focused on 736 ISGs (induced by TNF and identified by the Interferome database (17)) and studied the impact of DEX on the Log Fold Induction of these genes. As shown in **Figure 6C**, the reduced expression by DEX was found to be stronger in $GR^{wt/wt}$ mice compared to $GR^{dim/dim}$ mice (35% and 28% respectively) suggesting poorer repression of ISGs by DEX in $GR^{dim/dim}$ mice. Next, we questioned whether DEX was able to significantly repress TNF-induced ISGs in $GR^{wt/wt}$ mice, but not in $GR^{dim/dim}$ mice and found a list of 93 genes following this pattern (**Figure 6D and Supplemental File SF6**). Interestingly, this list contains genes coding for proteins important in the induction of necroptotic cell death, namely *Ripk3*, *Zbp1* and *Mlkl*.

The expression levels of these three genes, as determined by RNAseq are depicted in **Figures 6E** (*Ripk3*) **and Supplemental File SF6** (*Zbp1* and *Mlkl*). Based on Figure 6E, it is clear that *Ripk3* is significantly higher expressed in $GR^{dim/dim}$ mice compared to $GR^{wt/wt}$ mice in basal conditions and after stimulation with an equal dose of TNF (12.5 µg/mouse) in both groups . Moreover, expression of *Ripk3* mRNA is less repressed by DEX pretreatment in these mice. The function of these genes is strictly linked to necroptotic cell death (29). The induction of RIPK3 protein was measured by IHC on ileum sections (**Figure 6F)** and appeared more pronounced in the gut of $GR^{dim/dim}$ compared to $GR^{wt/wt}$ mice. The staining was particularly strong in crypts as indicated by white arrows. Supporting a role for necroptosis, the extreme sensitivity for TNF-induced lethal SIRS of $GR^{dim/dim}$ mice was reverted by pretreatment with Nec1s (29), a specific necroptosis inhibitor (**Figure 6G**). These data combined, suggest that necroptosis is a contributing pathway which is stronger induced by TNF in $GR^{dim/dim}$ mice, potentially because the *Ripk3*, *Zbp1* and *Mlkl* genes are stronger induced in these mice.

Discussion

GCs are powerful in protecting against the TNF-induced lethal shock model (7) but the mechanism of protection is not clear. Here, we describe that DEX confers protection against TNF in $GR^{wt/wt}$ mice, yet fails to do so in $GR^{dim/dim}$. Both $GR^{dim/dim}$ and $GR^{VillinKO}$ mice exhibit a stronger response to TNF with gut barrier leakiness and DEX failed to provide protection against TNF in both these mutant mice. $GR^{dim/dim}$ mice exhibit more structural damage and cell death of IECs in response to TNF.

RNAseq analysis on IECs of $GR^{wt/wt}$ and $GR^{dim/dim}$ mice in basal conditions, revealed an unexpected and strong interferon signature in $GR^{dim/dim}$ mice. The phosphorylation state of STAT1 in $GR^{dim/dim}$ mice implied that STAT1 is more transcriptionally active. The enhanced expression of *Stat1* and ISGs depends on the GR, since the same ISG signature could be seen in IECs of $GR^{VillinKO}$ mice and, importantly, appeared to be IEC specific. Interestingly, the ISG signature in IECs of $GR^{dim/dim}$ mice was confirmed by a proteome-wide MS experiment: 32 proteins were identified as significantly upregulated, including 17 interferon stimulated proteins such as STAT1.

The RNAseq analysis showed that in basal conditions, 664 genes were DE in $GR^{dim/dim}$ mice of which 460 were upregulated and 204 downregulated. This result is in contrast with the genome wide expression profiling by Frijters *et al.*, where no DE genes were found in liver samples of $GR^{wt/wt}$ and $GR^{dim/dim}$ mice. Based on their findings, the authors suggested that the GR dim mutation itself does not cause differential gene regulation (13). The discrepancy between their liver and our IEC results might be explained by the fact that local GC production in the gut could lead to GR dimer formation even in the absence of exogenous ligand. It is important to note that recent studies in unchallenged mice suggest that in the absence of synthetic ligand, the DNA-bound GR almost exclusively resides in its monomer form and that virtually the complete population of GR forms GR dimers upon injection of pharmacological doses of ligand (14). Hence, it is plausible that in organs where GCs are produced locally, CS levels rise to a level sufficient to support GR dimerization, leading to transactivation or

repression of particular GR dimer-sensitive target genes. This mechanism may be playing a role in the IECs, as these are known to produce CS (19).

As an additional explanation for the gut-specificity of this ISG signature, the role of the gut microbiota was investigated. Elimination of this factor by antibiotics strongly (but not completely) reduced expression of *Stat1* and other ISGs, and led to some, albeit incomplete, protection against TNF-induced lethality in $GR^{dim/dim}$ mice. These results suggest a link between ISG signature and TNF sensitivity, which is in line with earlier data using IFN receptor KO mice (3). The fact that antibiotics only partly protect against TNF, and do not completely revert the $GR^{dim/dim}$ sensitivity for TNF, suggests that either the elimination of gut flora is incomplete, e.g. leaving certain resistant bacteria, viruses and fungi intact, or that the contribution of ISGs is only partial. STAT1, however, is a central player in TNF-induced lethal SIRS, as well as gut permeability, as we show using $STAT1^{-/-}$ mice. Unfortunately $GR^{dim/dim}STAT1^{-/-}$ mice appeared not viable due to an unknown cause. Tofacitinib, a JAK/STAT1 inhibitor, like antibiotics, led to a significant, yet incomplete reversal of the TNF sensitivity of $GR^{dim/dim}$ mice.

Our data suggest that endogenous GCs are (i) induced in a gut flora-dependent way as a result of the ISG signature which includes the steroidogenic *Cyp11a1* and *Cyp11b1* genes, but (ii) also repress the ISGs via GR dimers. Since STAT1 is a central core node regulator of ISGs, it is conceivable that GR dimers block ISGs at the level of STAT1. Activated STAT1/STAT1 homodimers or STAT1/STAT2 heterodimers translocate to the nucleus where they participate in the regulation of the expression of ISGs (26). GCs are known to modulate IFN signaling at different levels. First, GCs repress the type I IFN production leading to reduced expression of ISGs (30, 31). Second, GCs inhibit STAT1 activation at therapeutic but also physiological levels by repressing its mRNA and protein expression (32). Third, STAT1 phosphorylation and occupancy of ISRE sequences in the DNA is actively inhibited by GC treatment (33–35). Inhibition of the STAT1 system including expression, phosphorylation and occupancy of ISREs, might be an important part of the anti-inflammatory capacities of GCs (34).

However, we found no such evidence in $GR^{dim/dim}$ mice. Fourth, increased *Stat1* expression could result from binding of GR dimers to GRE elements with nGRE activity leading to downregulation of gene expression. Several GRE elements have recently been described in the mouse *Stat1* gene (36). Fifth and of interest here, GR dimers inhibit STAT1 transcription via so called IR-nGREs (consensus sequence: $CTCC(N)_{0-2}GGAGA$), first described by Surjit *et al*., and present in the promoter of many genes, leading to transcriptional repression via binding of GR dimers (15). *In silico* analysis of the STAT1 promoter predicted two IR-nGRE elements (IR nGRE1 & IR nGRE2). Although we found no difference in GR occupancy on these elements between naïve $GR^{wt/wt}$ and $GR^{dim/dim}$ mice, we clearly found GR recruitment after DEX injection in $GR^{wt/wt}$ mice, but not in $GR^{dim/dim}$ mice, suggesting a dimer-specific interaction. It is also important to note that although Surjit *et al.* clearly showed that DEX-induced IR-nGRE mediated repression was abolished in $GR^{dim/dim}$ mice, it is suggested that GR dimers are formed in an structurally alternative way on these elements (37). Sixth, since the genes that are downregulated by DEX in IECs in a GR dimer-dependent way appear to be strongly enriched in IRF1 and ISRE sequences, GR dimers may bind to IRF1 on the one hand or STAT1, STAT2 or IRF9 on the other hand, and form a transcriptionally inhibitory complex.

The genes coding for key enzymes of CS synthesis were found to be upregulated in naïve $GR^{dim/dim}$ mice, which is compatible with the fact that they are known in the Interferome database as ISGs (17). Antibiotics downregulate expression of these genes, and also downregulate IEC-specific production of CS. These data are in line with the hypothesis that IECs are stimulated by gut flora to produce ISGs, including genes leading to local CS production, which triggers GR dimers to suppress this ISG signature at the level of STAT1. Larsson *et al.* showed dramatic transcriptional responses to microbiota in all segments of the gut by comparing the gene expression profile of germ-free and conventionally raised wildtype mice (38). Similar to other studies, Larsson *et al.* observed a significant microbial induction of genes related to immunity (39). Moreover, sensing of microbial products by various receptors triggers ISG expression via IFN-β and IFN-α production (22).

Interferons are known to prime cells for subsequent inflammatory triggers (40). By RNAseq in IECs of $GR^{wt/wt}$ and $GR^{dim/dim}$ mice, we found that TNF induces ISGs, and that an equal dose in both groups of mice led to higher LFCs of ISG expression in $GR^{dim/dim}$ mice. “Interferon Signaling” and “Activation of IRF” were the two most significant pathways predicted by IPA in $GR^{dim/dim}$ mice injected with a lethal dose of TNF compared to $GR^{wt/wt}$ mice injected with a lethal TNF dose. These data suggest that the increased sensitivity for TNF in $GR^{dim/dim}$ mice is based on an uncontrolled induction of ISGs, not by a priming *sensu stricto*.

Finally, to understand why $GR^{dim/dim}$ mice are not protected against TNF-induced permeability and lethality by exogenous GCs, we studied the impact of DEX on TNF-induced changes in IECs and performed a genome wide expression profiling via RNAseq in IECs of DEX and DEX/TNF treated $GR^{wt/wt}$ and $GR^{dim/dim}$ mice. DEX inhibits several TNF-induced physiological changes in a dimer-dependent way, namely gut permeability, gut damage and cell death. The transcription factor binding motifs found in the genes repressed by DEX in a dimer-specific way were ISRE and IRF elements only. This suggests a poor repression of ISGs in $GR^{dim/dim}$ mice, which was confirmed by the lower impact of DEX on the repression on TNF-induced ISGs in $GR^{dim/dim}$ compared to $GR^{wt/wt}$ mice. Whether GR dimers limit the expression of ISGs through inhibition of STAT1 or at the level of each individual ISG via their IRF or ISRE element is so far unclear. We identified 93 genes induced by TNF, but of which induction was significantly prevented by DEX in a $GR^{wt/wt}$-specific way. In this group, we found *Ripk3*, *Zbp1* and *Mlkl* which are important mediators of necroptosis, a form of cell death recently associated with SIRS (29, 41). Zbp1, also known as DAI, is a molecule known to be induced by microbial/viral stimuli and is able to lead to necroptosis, in combination with Ripk3, in the absence of Ripk1 (42–44). Mlkl is the major target of the Ripk1/Ripk3 heterodimer or Zbp1/Ripk3 heterodimer and cleavage of Mlkl eventually leads to necroptotic cell death. Clearly, these molecules behave like ISGs and are significantly higher expressed in and less repressed by DEX in $GR^{dim/dim}$ mice . Therefore, a more outspoken induction of necroptosis by TNF as well as a lack of repression of cell death by DEX

in the IECs of $GR^{dim/dim}$ mice might form an attractive explanation of the phenotypes discussed in this paper.

In conclusion (**Figure 6H**), we reveal a hitherto unknown physiological pathway in the epithelial cells of the gut involving microbiota-stimulated ISGs expression via STAT1. The family of ISGs contains *Cyp11a1* and *Cyp11b1*, which code for essential enzymes involved in local CS production. CS subsequently stimulates GR dimer formation and inhibits *Stat1* and other ISG gene expressions. Interestingly, genes coding for proteins involved in cell death also belong to the family of ISGs, namely *Ripk3*, *Zbp1* and *Mlkl*. Expression of these genes, as well as cell death, is inhibited by CS pretreatment. TNF stimulates STAT1 and ISGs, including these cell death promoting genes. In the absence of GCs or GR dimers, the induction of ISGs by microbiota and TNF is no longer properly controlled, leading to excessive TNF-induced cell death, permeability and lethality. Our work suggests that GCs protect against acute TNF-induced inflammation, predominantly in IECs and by a dimer-dependent repression of microbiota- and TNF-induced ISGs, including the master regulator STAT1.

Which microbes are involved in this pathway, and whether this pathway is relevant in other mammals than mice, given their coprophagy behavior, is not known. Moreover, since the role of TNF in real human pathologies may be different than in a mouse model of TNF-induced acute inflammation, and given the fact that, based on alternative splicing and alternative start codon use, (as elegantly shown by Cidlowski and his team), several different GR proteins, with different functions are expressed in different tissues during diseases, the impact of our findings in other mouse models and in human patients will need further investigation (45).

Methods

Mice. $GR^{dim/dim}$ mice were generated by Reichardt *et al.* and kept on an FVB/N background (11). Heterozygous $GR^{dim/wt}$ mice were intercrossed to generate $GR^{wt/wt}$ and $GR^{dim/dim}$ homozygous mutant

mice. All offspring was genotyped by PCR on genomic DNA isolated from toe biopsies. $GR^{flox/flox}$ mice (46) were crossed with Villin Cre transgenic mice (47), and the offspring intercrossed to generate $GR^{VillinKO}$ and $GR^{flox/flox}$ mice, all in a C57BL6/J background. C57BL6/J wildtype mice and $STAT1^{-/-}$ were purchased from Janvier and the Jackson Laboratory, respectively. Mice were kept in individually ventilated cages under a 12 hour dark/light cycle in a conventional and specific pathogen free (SPF) animal facility and received food and water *ad libitum*. All mice were used at 8-12 weeks of age. All animal experiments were approved by the ethical committee for animal welfare of the Faculty of Sciences, Ghent University.

Reagents. Recombinant mouse TNF was produced in *E. Coli* and purified to homogeneity in our laboratories. TNF had a specific activity of $1.2x10^8$ IU/ mg and no detectable endotoxin contamination. Dexamethasone or DEX (D-4902) and FD4 Fluorescein isothiocyanate (FITC)–dextran (FD4-1G, Mw 3,000-5,000 Da) were purchased from Sigma-Aldrich NV. Recombinant TNF, DEX and FITC-dextran were diluted in pyrogen-free PBS. Tofacitinib (CP-690550) Citrate (S5001; Shelleckchem Inc.) was diluted in 2% Tween 80 with 0.5% methylcellulose diluted in PBS. Nec1s is a necroptosis inhibitor was diluted in DMSO and was used as recently described (48).

Injections and sampling. All injections were given intraperitoneally except for Nec1s experiments where intravenous injection were used. Injection volumes were always adapted to the bodyweight of the mice. In lethality experiments, lethal response was followed until no further deaths occurred. FITC-dextran and Tofacitinib were administered via oral gavage. Blood was taken via cardiac puncture after sedation of the mice with a ketamine/xylazine solution (Sigma-Aldrich NV). To obtain mouse serum, samples were allowed to clot overnight at 4°C. The next day the cloth was removed and samples were centrifuged at 14,000 rpm for 3 minutes. Serum samples were stored at -20°C. For sampling of different organs and IECs, the mice were killed by cervical dislocation at indicated time points. IEC samples for RNA isolations were prepared as follows: Ileum was dissected, extensively flushed with PBS and incubated with lysis buffer (732 6802; Biorad) supplemented with 2-

mercaptoethanol on ice for 5 minutes. Samples were then snapfrozen in liquid nitrogen. IEC samples for western blot analysis were also snapfrozen. For histology, a piece of ileum was fixed in 4% paraformaldehyde and embedded in paraffin by a standard protocol.

Intestinal permeability. An *in vivo* permeability assay was performed using FITC-dextran as described previously (4). Three hours after TNF challenge, 100 µl FITC-dextran (25 mg/ml in PBS) was administered by oral gavage. Five hours later, blood was collected in an EDTA coated tube and centrifuged at 500 g for 10 min. Plasma was collected and fluorescence was measured $\lambda_{exc}/\lambda_{em}$ = 488/520 nm.

Tissue sections, histology and immunohistochemistry. Tissue sections of 4 µm were cut and stained with hematoxylin & eosin (H&E) using standard protocols. Pictures were taken with an Olympus Bx51 Light microscope (40x). Tissue damage was quantified by four neutral observers using the necrotizing enterocolitis scoring system published and validated by Halpern *et al.* (28). The mean values of all estimations was used. Cell death was identified by the terminal deocynucleotidyl-transferase-mediated deoxyuridine triphosphate nick-end labeling technique (TUNEL, Fluorescein In Situ Cell Death Detection Kit; Roche) according to the manufacturer's protocol.

Immunohistochemistry RIPK3. For immunochemistry, tissue sections were dewaxed, incubated in Dako antigen retrieval solution (DAKO) at boiling temperature for 20 min in a Pick cell cooking unit, and cooled down for 2.5h. Blocking buffer (5% goat serum in PBT, i.e. PBS, 0.1% Bovine Serum Albumin and 1% Triton X-100) was added to the slides for 30min at room temperature. Primary antibody against RIPK3 (ADI-905-242-100; Enzo Life Sciences) was diluted 1:200 in PBT and incubated overnight at 4°C. Slides were then incubated with secondary antibody (goat anti-rabbit labeled (E0432; DAKO- 1:500 in blocking buffer) and streptavidin-Alexa-fluor568; (S11223- 1:500 in blocking buffer)). Counterstaining was done with Hoechst reagent (Sigma-Aldrich NV-1:1,000 in PBS). Fluorescence microscopy was performed using a Zeiss Axioscan Z.1.

qPCR analysis. RNA was isolated with the RNeasy Mini kit (Qiagen) according to the manufacturer's instructions. RNA concentration was measured with the Nanodrop 1000 (ThermoFisher Scientific) and 300-1,000 ng RNA was used to prepare cDNA with Superscript II (Invitrogen). qPCR was performed using the Roche LightCycler 480 system (Applied Biosystems). The best-performing housekeeping genes were determined by Genorm (49). Results are given as relative expression values normalized to the geometric mean of the housekeeping genes. Primers used for qPCR are depicted in **Table I**.

RNA sequencing analysis of IEC samples. Total RNA was isolated with the RNeasy Mini kit (Qiagen) according to the manufacturer's instructions. Biological triplicates were used for every condition. RNA concentration was measured and RNA quality was checked with the Agilent RNA 6000 Pico Kit (Agilent Technologies) and sequenced on a Illumina Genome Analyzer IIx. Data was mapped to the mouse (mm10) reference genome transcriptome with tophat2 (50). Only uniquely mapped reads were retained. Gene level read counts were obtained with the HTSeq python package. Differential gene expression was assessed with the DESeq2 package and the false discovery rate (FDR) was set at the 1% level. Functional analysis of differentially expressed gene lists was performed via Ingenuity Pathway analysis or IPA. Part of the comparison between different TNF conditions was also done using IPA. Motif finding for multiple motifs or *de novo* motif finding was performed using the HOMER software. We used the promoter region (start offset: -500, end offset: default) to search for known motifs and *de novo* motifs of length 8, 10, 12, 14 and 16. Searching for specific motifs in a set of sequences was done with the meme suite. Visualizations were made using the R software. The data of these RNA sequencing experiments are available at NCBI via accession number GSE 113691.

Proteomics sample preparation, LC-MS/MS analysis and data analysis. See Supplemental Materials and Methods.

Western blot analysis. For the detection of STAT1 and pSTAT1, protein was isolated out of IECs (lysis buffer with 0.1% SDS, 150 mM NaCl, 50 mM Tris pH 8, 1% NP-40, 0.5% deoxycholate, 0.5 mM EDTA

supplemented with protease and phosphatase inhibitor cocktails from Roche). Protein samples containing 50 µg protein were separated by electrophoresis in a 10% gradient SDS polyacrylamide gel and transferred to nitrocellulose membranes (pore size 0.45 µm). After blocking the membranes with 1:2 dilution of Starting Block/PBST0.1% (ThermoFisher Scientific), membranes were incubated overnight at 4°C with primary antibodies against pSTAT1 (1:1,000; 9167S; Cell Signaling), STAT1 (1:1,000; D1K9Y; Cell Signaling) and ACTIN (1:5,000; 691002; Bio-Connect). Blots were washed with PBST0.1% and then incubated for 1 hour at room temperature with anti- rabbit antibody (1:10,000; 926-32211; Li-cor) and anti-mouse antibody (1:10,000; 926-32220; Li-cor). Immunoreactive bands were detected using the Odyssey Infrared Imager (Li-cor) and quantified using Image Studio Lite Version 4.0.

Isolation of Mouse IECs and Chromatin Immunoprecipitation (ChIP). IECs were isolated as previously described (51). Briefly, whole small intestines were cut into pieces and incubated at 37°C in Dulbecco's modified Eagle medium (DMEM) containing 5% fetal calf serum (FCS) and 1 mM dithiothreitol (DTT) for 30 minutes. The remaining tissue was incubated in PBS containing 1.5 mM EDTA for an additional 10 minutes. Supernatant was filtered using a 70 µm cell strainer, centrifuged for 5 min at 400 g, and the cell pellet was resuspended in optimem (Gibco). The ChIP assay protocol was based on Schmidt *et al.* (52). Mouse IECs diluted in optimem were immediately fixed in 1% formaldehyde for 10 min at room temperature while gently shaking. The reaction was stopped by adding 125 mM glycine for 10 min with shaking. Cells were washed with PBS and pellets were lysed in lysis buffer supplemented with protease inhibitors (0.1% SDS, 1% Triton X-100, 0.15M NaCl, 1mM EDTA and 20 mM Tris pH 8). Lysates were sonicated using a Bioruptor instrument (Diagenode) for 30 min with 30 seconds on/30 seconds off intervals. Supernatant was taken and used as input and for immunoprecipitation. nProtein sepharose beads (GE Healthcare) were washed in incubation buffer (0.15% SDS, 1% Triton X-100, 0.15M NaCl, 1mM EDTA, 20mM HEPES) and incubated with 1 µg BSA for 2 hours. Samples were first incubated with 5 µg anti-GR H300 antibody (sc-8992; Santa Cruz) or IgG control (10500C; Invitrogen) and then added to the blocked beads overnight. All incubations

were performed at 4°C while rotating. The next day, samples were extensively washed using spin columns with 0.35 µm pore size filters (MoBiTec) and eluted with elution buffer (1% SDS and 0.1 M $NaHCO_3$) for 20 min. Next, supernatant was incubated with 200 mM NaCl, 20 µg/ml RNase A (Qiagen) and 1 mg/ml proteinase K (VWR International) for 2 hours at 55°C and for 5 hours at 65°C. DNA was purified with Qiaquick PCR purification kit according to the manufacturer's protocol (Qiagen). qPCR was performed using the Roche LightCycler 480 system (Applied Biosystems). Following primers for the STAT1 promoter were used: *IR-nGRE1* (fwd 5'-CCTGCTGCTCTCAAGGTT-3'; rev 5'-TGGTTGTCACTGCCTCGTACTT-3'), *IR-nGRE2* (fwd 5'-TGAAGCAGGCATCTGAGGG-3'; rev 5'-CGAAGGTGGAAGAGTGGGAG-3'). Normalization of the ChIP data was done based on a method described by Haring *et al.*, as follows (53): for each sample, data with GR-specific H300 antibody or IgG control were normalized to an input sample. This input sample is indicative for the presence and amount of chromatin used in the ChIP reaction. This DNA sample yields a PCR product with all primer sets used.

Antibiotics-mediated depletion of commensal bacteria. Mice were kept in individual cages and treated with a dilution of a 100 mg/l ciprofloxacin (Sigma-Aldrich NV), 500 mg/l ampicillin (Sigma-Aldrich NV), 500 mg/l metronidazole (Sigma-Aldrich NV), and 250 mg/l vancomycin (Duchefa Biochemie) solution in their drinking water for three weeks. After two weeks, the presence of microflora was determined by culturing fecal samples in brain heart infusion (Becton-Dickinson) and thioglycollate medium (Sigma-Aldrich NV).

Measuring corticosterone produced by IECs using ileum explants. Mice were anesthetized with a ketamine/xylazine solution and perfused via the *vena cava inferior* with PBS supplemented with heparin to remove contamination of peripheral tissues by adrenal-produced corticosterone (CS). After perfusion, ileum samples of equal size were collected and flushed with PBS in order to remove remaining feces. Next, ileum samples were cut longitudinally and in small pieces which were incubated in optimem (Gibco) at 37°C. Supernatant of ileum explants was collected after five hours

and CS levels were determined with the Corticosterone EIA Kit (Arbor Assays) and according to the supplier's standard protocol.

Statistics. For dose curve experiments, 95% confidence intervals were calculated for the LD_{50} of each group by GenStat Fifteenth Edition. Statistics on survival curves were performed using the Log-rank test but a Chi^2 test was used in order to determine differences between final outcome. Statistical significance of differences between groups was determined by two-tailed Student's t tests, one-way ANOVA or two-way ANOVA tests with 95% confidence intervals. All data, except RNAseq data, are expressed as mean ±SEM and analyzed using Graphpad Prism software. A p-value less than 0.05 was considered significant.

Study approval. All experiments described in this paper have been approved by the ethical committee of the Faculty of Sciences of Ghent University.

Author contributions

M.B., K.V., S.T., M.E., S.V., F.T., K.D., J.S., J.V., L.V.W., R.D.R., N.T., F.I. and R.E.V. performed and guided experimental work. C.L. supervised the design and performances of the experiments. S.T. performed the analysis of RNA sequencing data and made graphical overviews for the manuscript. M.E., K.D. and J.S. provided technical assistance. H.M.R. and J.T. provided the $GR^{dim/dim}$ and $GR^{flox/flox}$ respectively. R.B., P.V., F.I. and K.D.B. provided other essential tools and useful comments and suggestions. M.B. and C.L. wrote the manuscript.

Acknowledgements

The authors wish to thank Joke Vanden Berghe, Sara Van Ryckeghem and animal house caretakers for animal care. We also want to thank Lien Dejager and Filip Van Hauwermeiren for their help with isolations in intestinal permeability experiments. We acknowledge the VIB Nucleomics Core for RNA sequencing analysis and Marnik Vuylsteke for statistical assistance. We are grateful to Kelly Lemeire

for performing TUNEL stainings and IHC on tissue sections. Research in these laboratories was funded by the Agency for Innovation of Science and Technology in Flanders (IWT), the Research Council of Ghent University (GOA program), the Research Foundation Flanders (FWO Vlaanderen), COST action BM1402, and the Interuniversity Attraction Poles Program of the Belgian Science Policy (IAP-VI-18). Funding from the DFG – ANR Tu 220/13-1, DFG, Collaborative Research Center 1149, C02/INST 40/492-1

References

1. Van Hauwermeiren F, Vandenbroucke RE, Libert C. Treatment of TNF mediated diseases by selective inhibition of soluble TNF or TNFR1. *Cytokine Growth Factor Rev.* 2011;22(5–6):311–319.

2. Billiet T, Rutgeerts P, Ferrante M, Van Assche G, Vermeire S. Targeting TNF-α for the treatment of inflammatory bowel disease. *Expert Opin. Biol. Ther.* 2014;14(1):75–101.

3. Huys L et al. Type I interferon drives tumor necrosis factor-induced lethal shock. *J. Exp. Med.* 2009;206(9):1873–82.

4. Van Hauwermeiren F et al. Safe TNF-based antitumor therapy following p55TNFR reduction in intestinal epithelium. *J. Clin. Invest.* 2013;123(6):2590–2603.

5. Van Hauwermeiren F et al. TNFR1-induced lethal inflammation is mediated by goblet and Paneth cell dysfunction. *Mucosal Immunol.* 2015;8(4):828–840.

6. Vereecke L et al. Enterocyte-specific A20 deficiency sensitizes to tumor necrosis factor-induced toxicity and experimental colitis. *J. Exp. Med.* 2010;207(7):1513–1523.

7. Libert C, Van Bladel S, Brouckaert P, Fiers W. The influence of modulating substances on tumor necrosis factor and interleukin-6 levels after injection of murine tumor necrosis factor or lipopolysaccharide in mice. *J. Immunother.* 1991;10(4):227–235.

8. Sacta MA, Chinenov Y, Rogatsky I. Glucocorticoid Signaling: An Update from a Genomic Perspective. *Annu. Rev. Physiol.* 2016;78(1):155–180.

9. Vandevyver S et al. Glucocorticoid receptor dimerization induces MKP1 to protect against TNF-induced inflammation. *J. Clin. Invest.* 2012;122(6):2130–2140.

10. Kleiman a. et al. Glucocorticoid receptor dimerization is required for survival in septic shock via suppression of interleukin-1 in macrophages. *FASEB J.* 2012;26(2):722–729.

11. Reichardt HM et al. DNA binding of the glucocorticoid receptor is not essential for survival. *Cell* 1998;93(4):531–541.

12. Watson LC et al. The glucocorticoid receptor dimer interface allosterically transmits sequence-specific DNA signals. *Nat Struct Mol Biol* 2013;20(7):876–883.

13. Frijters R et al. Prednisolone-induced differential gene expression in mouse liver carrying wild type or a dimerization-defective glucocorticoid receptor. *BMC Genomics* 2010;11(1):359.

14. Lim H-WW et al. Genomic redistribution of GR monomers and dimers mediates transcriptional response to exogenous glucocorticoid in vivo. *Genome Res.* 2015;25(6):836–844.

15. Surjit M et al. Widespread negative response elements mediate direct repression by agonist-liganded glucocorticoid receptor. *Cell* 2011;145(2):224–241.

16. Reichardt SD et al. Glucocorticoids enhance intestinal glucose uptake via the dimerized glucocorticoid receptor in enterocytes. *Endocrinology* 2012;153(4):1783–1794.

17. Rusinova I et al. INTERFEROME v2.0: An updated database of annotated interferon-regulated genes. *Nucleic Acids Res.* 2013;41(D1). doi:10.1093/nar/gks1215

18. Schneider WM, Chevillotte MD, Rice CM. Interferon-stimulated genes: a complex web of host defenses. *Annu. Rev. Immunol.* 2014;32:513–45.

19. Cima I et al. Intestinal epithelial cells synthesize glucocorticoids and regulate T cell activation. *J. Exp. Med.* 2004;200(12):1635–1646.

20. Abt MC et al. Commensal Bacteria Calibrate the Activation Threshold of Innate Antiviral Immunity. *Immunity* 2012;37(1):158–170.

21. Ganal SC et al. Priming of Natural Killer Cells by Nonmucosal Mononuclear Phagocytes Requires Instructive Signals from Commensal Microbiota. *Immunity* 2012;37(1):171–186.

22. Kawashima T et al. Double-Stranded RNA of Intestinal Commensal but Not Pathogenic Bacteria Triggers Production of Protective Interferon-β. *Immunity* 2013;38(6):1187–1197.

23. Oitzl MS, Reichardt HM, Joëls M, de Kloet ER. Point mutation in the mouse glucocorticoid receptor preventing DNA binding impairs spatial memory. *Proc. Natl. Acad. Sci. U. S. A.* 2001;98(22):12790–5.

24. Meraz M a et al. Targeted disruption of the Stat1 gene in mice reveals unexpected physiologic specificity in the JAK-STAT signaling pathway. *Cell* 1996;84(3):431–442.

25. Durbin JE, Hackenmiller R, Simon MC, Levy DE. Targeted disruption of the mouse Stat1 gene results in compromised innate immunity to viral disease. *Cell* 1996;84(3):443–450.

26. Akira S. Functional roles of STAT family proteins: lessons from knockout mice. *Stem Cells* 1999;17(3):138–146.

27. Cada D, Demaris K, Levien T, Baker D. Tofacitinib. *Hosp. Pharm.* 2013;48(5):413–424.

28. Halpern MD et al. Hepatic inflammatory mediators contribute to intestinal damage in necrotizing enterocolitis. *Am. J. Physiol. Gastrointest. Liver Physiol.* 2003;284(4):G695-702.

29. Takahashi N et al. RIPK1 ensures intestinal homeostasis by protecting the epithelium against apoptosis. *Nature* 2014;513(7516):95–9.

30. Dupont E et al. Influence of in vivo immunosuppressive drugs on production of lymphokines. *Transplantation* 1985;39:143–147.

31. Norbiato G, Bevilacqua M, Vago T, Clerici M. Glucocorticoids and interferon-alpha in the acquired immunodeficiency syndrome. *J. Clin. Endocrinol. Metab.* 1996;81(7):2601–6.

32. Hu X, Li W-PP, Meng C, Ivashkiv LB. Inhibition of IFN-gamma signaling by glucocorticoids. *J. Immunol.* 2003;170(9):4833–4839.

33. Flammer JR et al. The Type I Interferon Signaling Pathway Is a Target for Glucocorticoid Inhibition. *Mol. Cell. Biol.* 2010;30(19):4564–4574.

34. Schreiber S et al. Activation of signal transducer and activator of transcription (STAT) 1 in human chronic inflammatory bowel disease. *Gut* 2002;51(3):379–385.

35. Bhattacharyya S, Zhao Y, Kay TW, Muglia LJC. Glucocorticoids target suppressor of cytokine signaling 1

(SOCS1) and type 1 interferons to regulate Toll-like receptor-induced STAT1 activation. *Proc. Natl. Acad. Sci. U. S. A.* 2011;108(23):9554–9559.

36. He B, Cruz-Topete D, Oakley RH, Xiao X, Cidlowski JA. Human Glucocorticoid Receptor β Regulates Gluconeogenesis and Inflammation in Mouse Liver. *Mol. Cell. Biol.* 2015;36(5):714–30.

37. Hudson WH, Youn C, Ortlund EA. The structural basis of direct glucocorticoid-mediated transrepression. *Nat Struct Mol Biol* 2013;20(1):53–58.

38. Larsson E et al. Analysis of gut microbial regulation of host gene expression along the length of the gut and regulation of gut microbial ecology through MyD88. *Gut* 2012;61(8):1124–1131.

39. Hooper L V, Macpherson AJ. Immune adaptations that maintain homeostasis with the intestinal microbiota. *Nat. Rev. Immunol.* 2010;10(3):159–169.

40. Yarilina A, Park-Min K-H, Antoniv T, Hu X, Ivashkiv LB. TNF activates an IRF1-dependent autocrine loop leading to sustained expression of chemokines and STAT1-dependent type I interferon-response genes. *Nat. Immunol.* 2008;9(4):378–387.

41. Duprez L et al. RIP Kinase-Dependent Necrosis Drives Lethal Systemic Inflammatory Response Syndrome. *Immunity* 2011;35(6):908–918.

42. Dondelinger Y, Hulpiau P, Saeys Y, Bertrand MJM, Vandenabeele P. An evolutionary perspective on the necroptotic pathway. *Trends Cell Biol.* 2016;26(10):721–732.

43. Newton K et al. RIPK1 inhibits ZBP1-driven necroptosis during development. *Nature* 2016;540(7631):129–133.

44. Lin J et al. RIPK1 counteracts ZBP1-mediated necroptosis to inhibit inflammation. *Nature* 2016;540(7631):124–128.

45. Gross KL, Cidlowski JA. Tissue-specific glucocorticoid action: a family affair. *Trends Endocrinol. Metab.* 2008;19(9):331–339.

46. Tronche F, Kellendonk C, Reichardt HM, Schütz G. Genetic dissection of glucocorticoid receptor function in mice. *Curr. Opin. Genet. Dev.* 1998;8(5):532–538.

47. el Marjou F et al. Tissue-specific and inducible Cre-mediated recombination in the gut epithelium. *Genesis* 2004;39(3):186–193.

48. Takahashi N et al. Necrostatin-1 analogues: critical issues on the specificity, activity and in vivo use in experimental disease models. *Cell Death Dis.* 2012;3(11):e437.

49. Vandesompele J et al. Accurate normalization of real-time quantitative RT-PCR data by geometric averaging of multiple internal control genes. *Genome Biol.* 2002;3(7):RESEARCH0034.

50. Trapnell C, Pachter L, Salzberg SL. TopHat: Discovering splice junctions with RNA-Seq. *Bioinformatics* 2009;25(9):1105–1111.

51. Ruiz PA, Shkoda A, Kim SC, Sartor RB, Haller D. IL-10 gene-deficient mice lack TGF-beta/Smad signaling and fail to inhibit proinflammatory gene expression in intestinal epithelial cells after the colonization with colitogenic Enterococcus faecalis. *J. Immunol.* 2005;174(5):2990–9.

52. Schmidt D et al. ChIP-seq: Using high-throughput sequencing to discover protein-DNA interactions. *Methods* 2009;48(3):240–248.

53. Haring M et al. Chromatin immunoprecipitation: Optimization, quantitative analysis and data normalization. *Plant Methods* 2007;3(1). doi:10.1186/1746-4811-3-11

Tables

Gene	Forward primer (5'-3')	Reverse primer (5'-3')
Rpl	CCTGCTGCTCTCAAGGTT	TGGTTGTCACTGCCTCGTACTT
Gapdh	TGAAGCAGGCATCTGAGGG	CGAAGGTGGAAGAGTGGGAG
Hprt1	AGTGTTGGATACAGGCCAGAC	CGTGATTCAAATCCCTGAAGT
Ubc	AGGTCAAACAGGAAGACAGACGTA	TCACACCCAAGAACAAGCACA
Villin	TCAAAGGCTCTCTCAACATCAC	AGCAGTCACCATCGAAGAAGC
Irf8	AGACCATGTTCCGTATCCCCT	CACAGCGTAACCTCGTCTTCC
Irf1	ATGGAAACCCCGAAACCGC	GATATTTCCAGTGGCCTGGA
Ifit1	CTGAGATGTCACTTCACATGGAA	GTGCATCCCCAATGGGTTCT
Ifit2	ATCTCTCCCTACTCTGCCCTCCTA	GCGTATAAATCAGCAATCCCTTCA
Stat1	TCACAGTGGTTCGAGCTTCAG	GCAAACGAGACATCATAGGCA
Cyp11a1	AGGTCCTTCAATGAGATCCCTT	TCCCTGTAAATGGGGCCATAC
Cyp11b1	AACCCAAATGTTCTGTCACCAA	CAAAGTCCCTTGCTATCCCATC

Table I: Primer sequences used for qPCR.

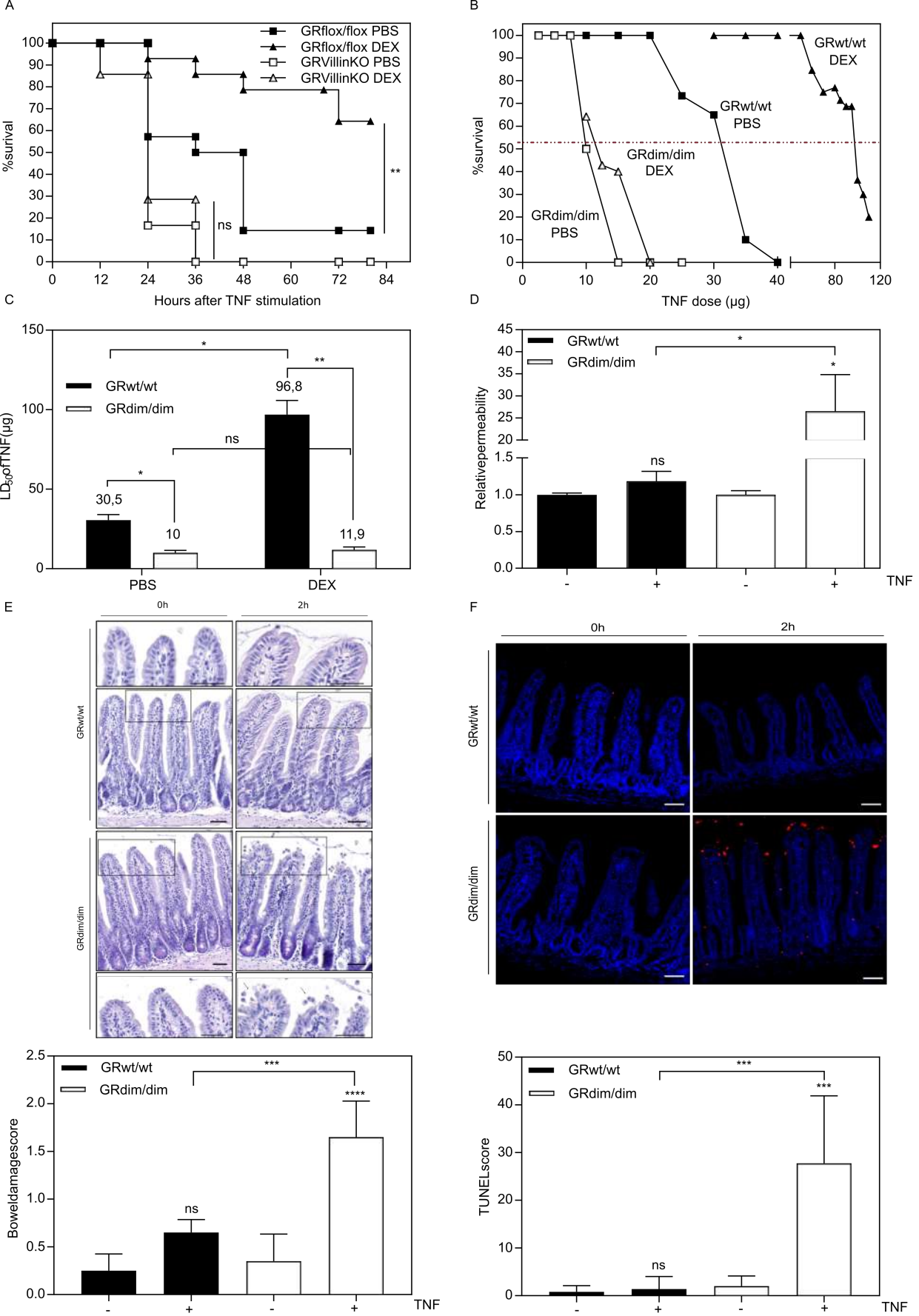

Figure 1: IEC GR and GR dimers play an essential role in the protection against TNF-induced lethality, gut permeability, damage and cell death. (A) GRflox/flox and GRVillinKO mice were pre-treated with PBS or with 10 mg/kg DEX. 30 min later, mice were injected with 35 µg of TNF and lethality was monitored. GRflox/flox mice (n=14 per group) are depicted in black squares (PBS) and triangles (DEX) and GRVillinKO mice (n=7 per group) in white squares (PBS) and triangles (DEX). p- values for survival curves were analyzed with a Logrank test (combined data of two independent experiments). **(B)** TNF dose-response curves of GRwt/wt (black) and GRdim/dim (white) mice pre-treated with PBS (squares) or with 10 mg/kg DEX (triangles) for 30 min (n= 8-10 per group; combined data of two independent experiments). **(C)** LD50 values of TNF are depicted on top of each bar for each group. 95% confidence intervals were calculated for the LD50 of each group. **(D-F)** GRwt/wt and GRdim/dim mice were injected with PBS or 12.5 µg of TNF (n=10 per group; combined data of two independent experiments). Asterisks refer to significant differences compared to PBS control, unless indicated otherwise. **(D)** Relative permeability, 8h after TNF challenge, is based upon systemic appearance of orally gavaged FITC-dextran in plasma samples. Standard H&E **(E)** and TUNEL staining **(F)** on ileum samples 8h after TNF were scored in order to calculate a bowel damage and TUNEL score, respectively. Notice a perfect appearance of GRwt/wt villi but villi damage, shortening, cell death and loss of goblet cells in GRdim/dim as well as TUNEL signals at villi tops and crypts. Scale bars represent 50 µm. Bars represent mean ± SEM. p–values were calculated using two-way ANOVA tests. *** p≤ 0.001, ** p≤ 0.01, * p ≤ 0.05 and ns = not significant.

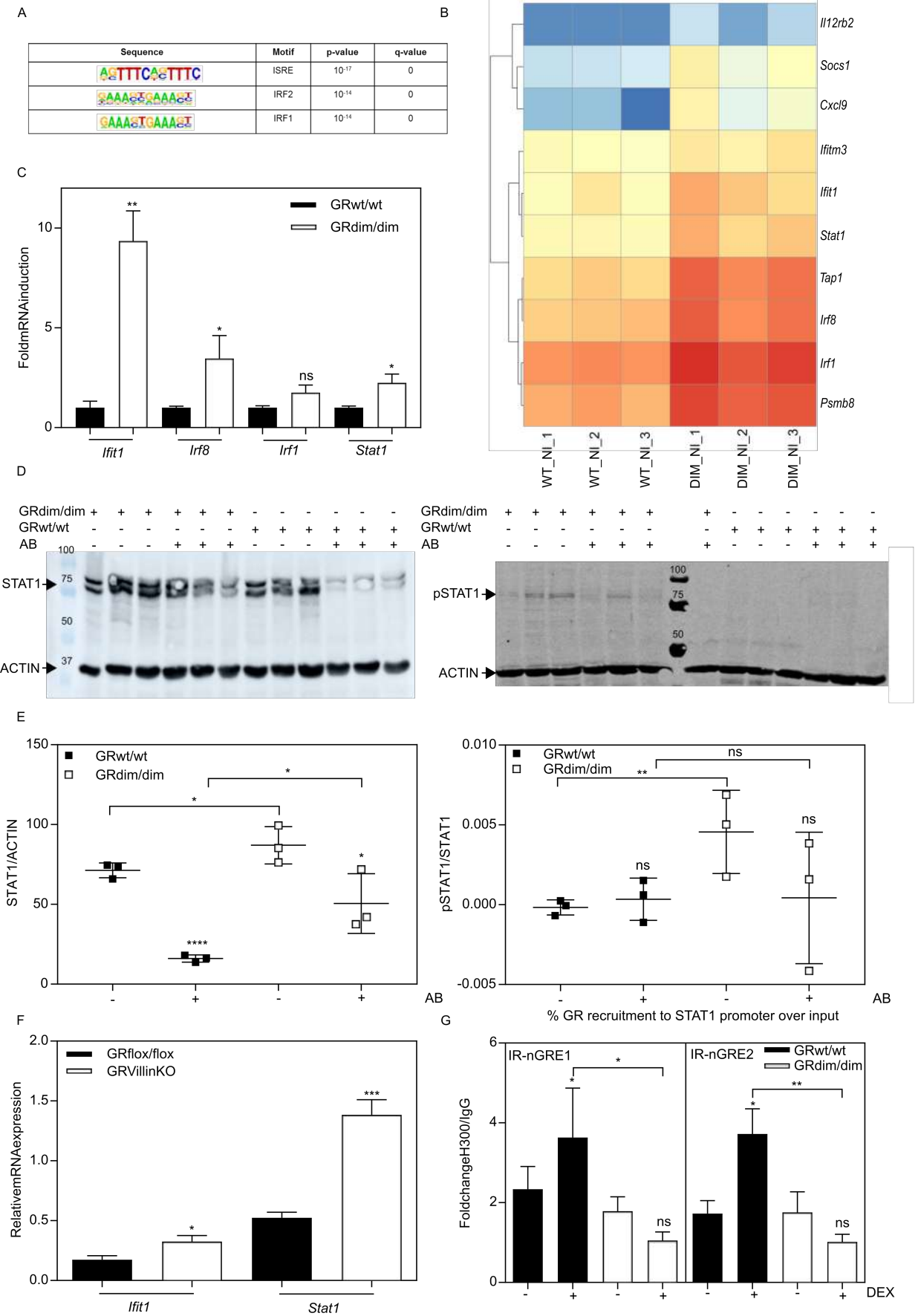

Figure 2: ISGs are expressed in the IECs of naïve GRdim/dim mice. (A-C) RNA sequencing of IECs of GRwt/wt (black) and GRdim/dim (white) mice (n= 3 per group). **(A)** HOMER motif analysis of differentially expressed (DE) genes in GRdim/dim compared to GRwt/wt mice. Motifs with highest rank and their p-value and q-value are displayed. **(B)** Heatmap of DE genes containing an ISRE and/or IRF-1 element. **(C)** Confirmation of RNAseq data with qPCR on independent new samples (n=3 per group). *Ifit1, Irf8, Irf1* and *Stat1* mRNA expression is shown as mean ± SEM. p–values were calculated using Student's t tests. **(D-F)** GRwt/wt and GRdim/dim mice received drinking water with or without antibiotics for 3 weeks after which IEC samples were taken (n= 3 per group). **(D)** STAT1 and pSTAT1 protein levels were analyzed via western blot using ACTIN as a loading control. **(E)** Relative STAT1 and pSTAT1 signal intensities were quantified and normalized to ACTIN and STAT1 levels respectively. p–values were calculated using two-way ANOVA tests. **(F)** *Stat1* and *Ifit1* mRNA expression was determined in IECs of GRflox/flox (black) and GRVillKO mice (white) via qPCR and is shown as mean ± SEM (n=5 per group). p–values were calculated using Student's t tests. (**G)** GR recruitment to two IR-nGRE sites in the STAT1 promoter (IR-nGRE1&2). GRwt/wt (black) and GRdim/dim (white) mice were treated with PBS or 10 mg/kg DEX for 2h (n=5 per group; combined data of three independent experiments). ChIP on IEC samples was performed against GR using an H300 antibody. Data were normalized to input for each sample and expressed as fold change of H300 to IgG control. p–values were calculated using two-way ANOVA tests. *** $p < 0.001$, ** $p \leq 0.01$, * $p \leq 0.05$ and ns = not significant.

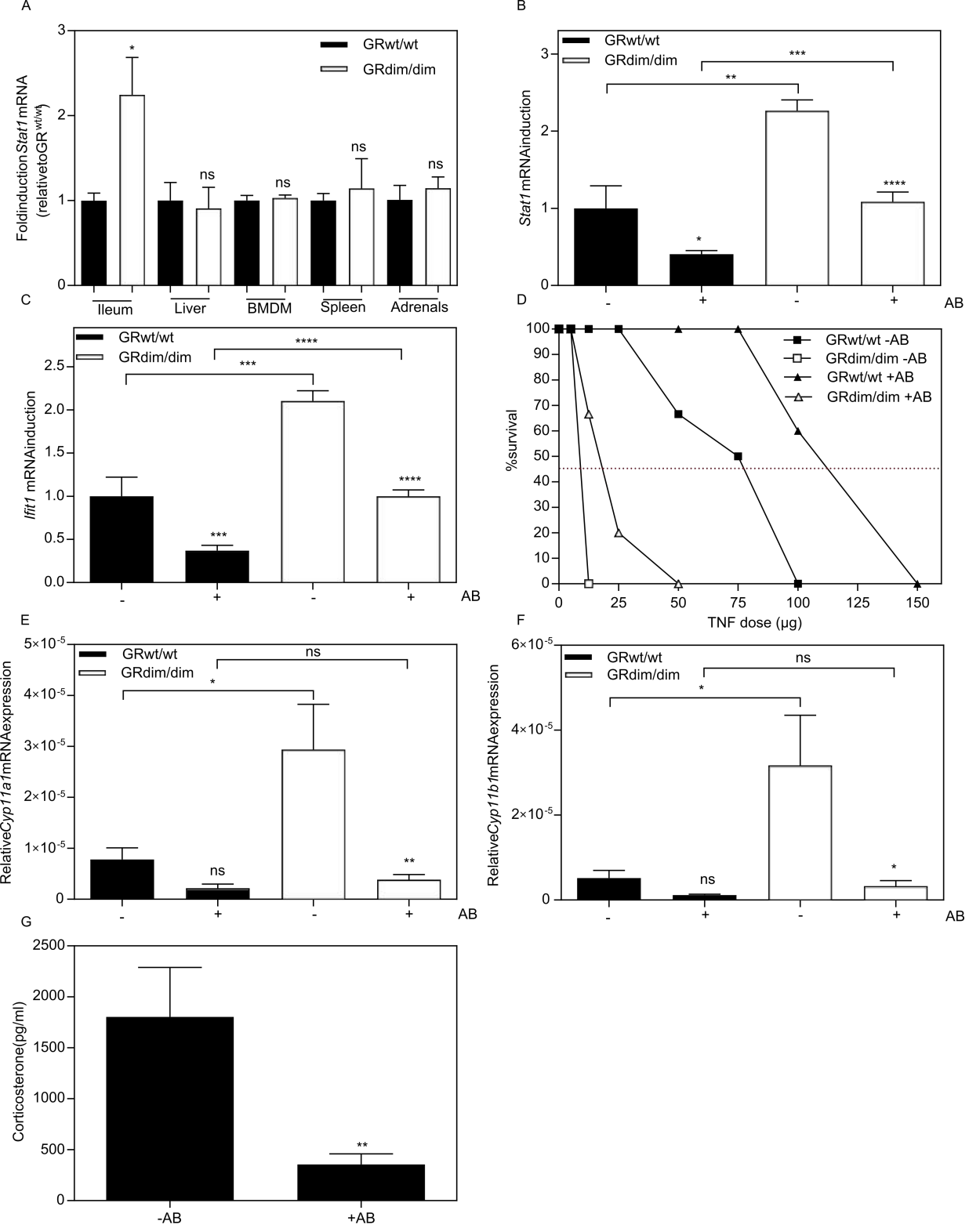

Figure 3: The gut microbiota determines the gut-specific ISG signature in GRdim/dim mice and local GC production.
(A) RNA was isolated from ileum, liver, bone marrow derived macrophages (BMDM), spleen and adrenal glands dissected from GRwt/wt (black) and GRdim/dim (white) mice. *Stat1* mRNA expression was analyzed via qPCR (n=4 per group). For each organ, different house-keeping genes were used for normalization and expression in GRwt/wt mice is set as 1. p–values were calculated using Student's t tests. **(B-E)** Effects of commensal bacteria depletion on ISG expression, pSTAT1 levels, TNF-induced lethality and GC production. GRwt/wt and GRdim/dim mice were treated with antibiotics (+AB) for three weeks. IECs were isolated and *Stat1* **(B)** and *Ifit1* **(C)** mRNA expression was determined via qPCR (n=8 per group, combined data of two independent experiments). p–values were calculated using two-way ANOVA tests. **(D)** TNF dose response curves of GRwt/wt and GRdim/dim mice treated with (triangle) or without (squares) antibiotics (n=4-6 per dose). **(E-G)** Effects of antibiotics on GC production. GRwt/wt and GRdim/dim mice were treated with antibiotics (+AB) for three weeks. *Cyp11a1* **(E)** and *Cyp11b1* **(F)** mRNA expression in IECs was determined via qPCR (n=4 per group). p–values were calculated using two-way ANOVA tests. (G) GC production in supernatant of ileum explants of GRwt/wt mice treated without (-AB) or with antibiotics (+AB) (n=5 per group). p–values were calculated by Student's t tests. All bars represent mean ± SEM. **** $p < 0.0001$, *** $p < 0.001$, * $p \leq 0.05$ and ns = not significant.

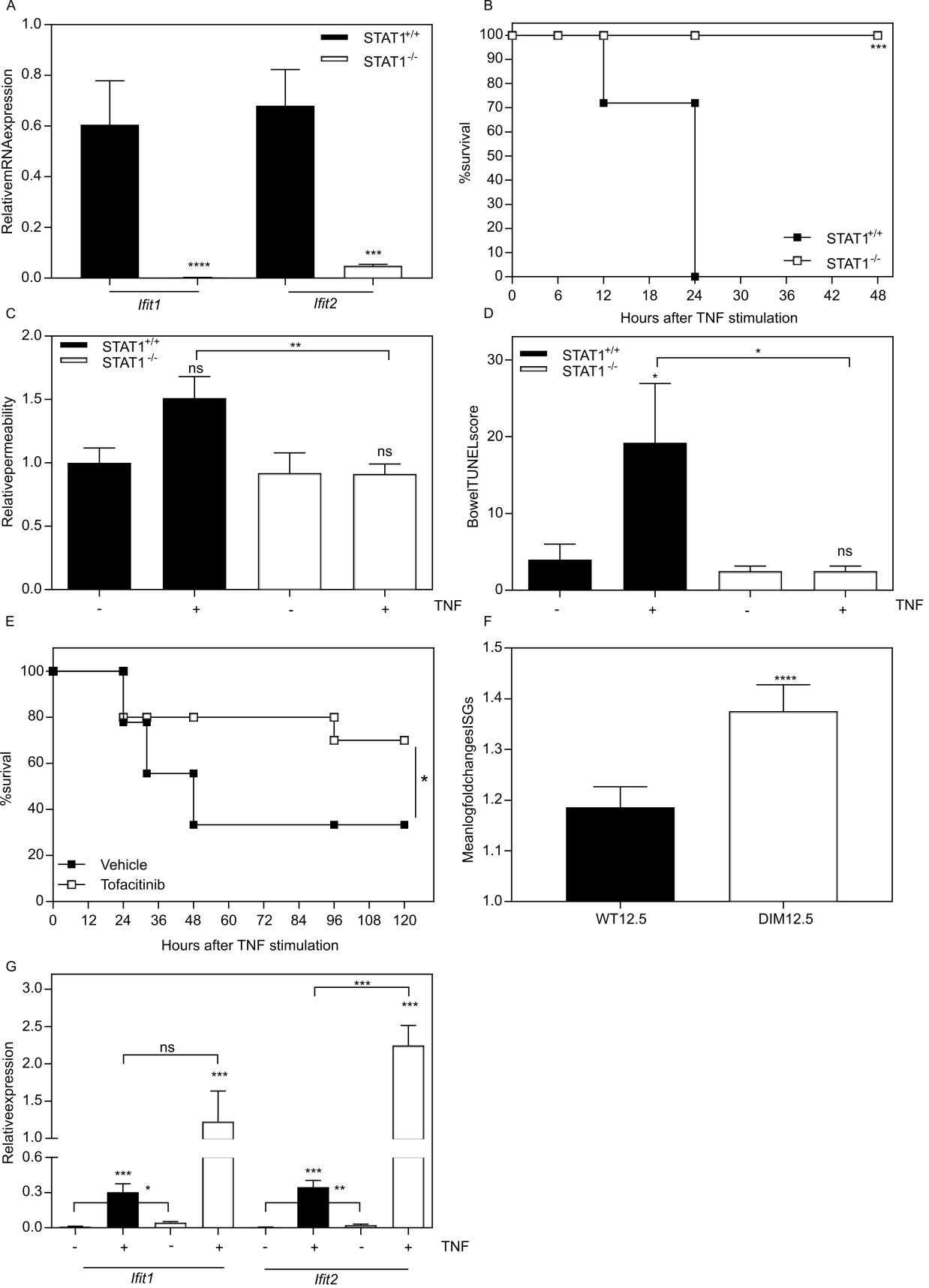

Figure 4: STAT1 is a master regulator of TNF sensitivity. (A) RNA was isolated from IECs of STAT1+/+ (black bars) and STAT1-/- mice (white bars). *Ifit1* and *Ifit2* mRNA expression levels were determined via qPCR (n=4 per group). p–values were calculated by Student's t tests. **(B-D)** STAT1 mediates TNF-induced lethality, intestinal permeability and cell death. **(B)** STAT1+/+ (black) and STAT1-/- (white) mice were injected with 35 µg TNF and survival was monitored (n=7 per group). Survival curves were analyzed with a Logrank test. **(C)** As a measure for intestinal permeability, systemic appearance of orally gavaged FITC-dextran in plasma samples was determined 8h after TNF injection in STAT1+/+ mice (PBS n=7; TNF n=14) and in STAT1-/- mice (PBS n=7; TNF n=15). **(D)** TUNEL staining was performed on ileum tissue sections and quantified (combined data of two independent experiments). p–values were calculated using two-way ANOVA tests. **(E)** STAT1 is an important regulator of GRdim/dim TNF sensitivity. Tofacitinib (100 mg/kg) or vehicle was given orally to GRdim/dim mice (n=10 per group; combined data of two independent experiments). Mice received Tofacitinib twice a day for 2 days before challenge (20 µg of TNF) and two times (1h before and 8h after) on the day of challenge. Survival was monitored and analyzed with a Logrank test. **(F)** Log Fold Changes of TNF-induced ISGs, detected by RNAseq, in IECs of GRwt/wt mice (black) or GRdim/dim mice (white) injected with 12.5 µg of TNF (n=4 per group). **(G)** *Ifit1* and *Ifit2* mRNA expression, measured by qPCR, in IECs of GRwt/wt and GRdim/dim, 8h after PBS or 12.5 µg TNF (n=4 per group). p–values were calculated using two-way ANOVA tests. All bars represent mean ± SEM. **** $p < 0.0001$, *** $p < 0.001$**, $p \leq 0.01$, * $p \leq 0.05$ and ns = not significant.

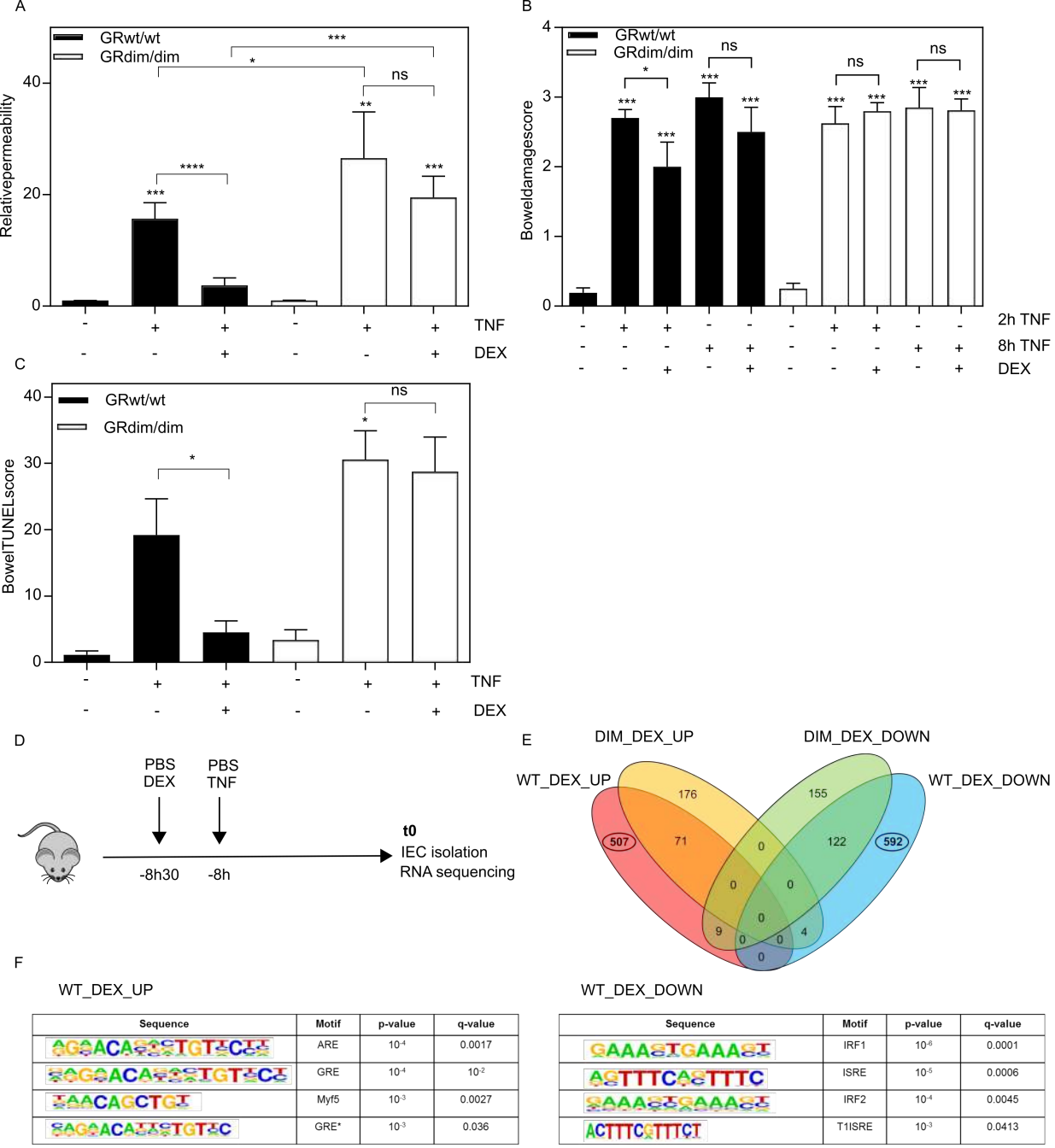

Sequence	Motif	p-value	q-value
	ARE	10^{-4}	0.0017
	GRE	10^{-4}	10^{-2}
	Myf5	10^{-3}	0.0027
	GRE*	10^{-3}	0.036

Sequence	Motif	p-value	q-value
	IRF1	10^{-6}	0.0001
	ISRE	10^{-5}	0.0006
	IRF2	10^{-4}	0.0045
	T1ISRE	10^{-3}	0.0413

Figure 5: Lack of protective effects of DEX against TNF-induced changes in the gut of GRdim/dim mice. (A-C) GRwt/wt (black) and GRdim/dim (white) mice were pre-treated with vehicle or 10 mg/kg DEX for 30 min followed by challenge with 50 µg or 12.5 µg of TNF respectively. **(A)** 8h after TNF challenge, systemic concentrations of FITC-dextran in plasma were determined after oral gavage and reflect relative intestinal permeability (n=12-20 per group; combined data of three independent experiments). **(B)** Ileum was sampled 2h and 8h after TNF injection (n=5 per group), stained with H&E and bowel damage scores determined. **(C)** Sections were stained for TUNEL and quantified. All bars represent mean ± SEM and p-values were calculated using two-way ANOVA tests. **(D-F)** RNAseq results of IECs of GRwt/wt and GRdim/dim mice pretreated with 10 mg/kg DEX or PBS, followed 30 min later by a lethal dose of TNF (50 µg for GRwt/wt and 12.5 µg for GRdim/dim mice) or PBS. **(D)** Overview of the experimental set-up. For all groups n=3 per group. **(E)** Venn diagram of differentially expressed genes upon DEX treatment compared to PBS-stimulated conditions. **(F)** Overview of the most significant transcription factor-binding motifs found enriched in the DEX-induced (left panel) and DEX-reduced (right panel) genes in GRwt/wt mice, using HOMER. Motifs with the highest rank and their p-value and q-value. **** $p < 0.0001$, *** $p < 0.001$**, $p \leq 0.01$, * $p \leq 0.05$ and ns = not significant.

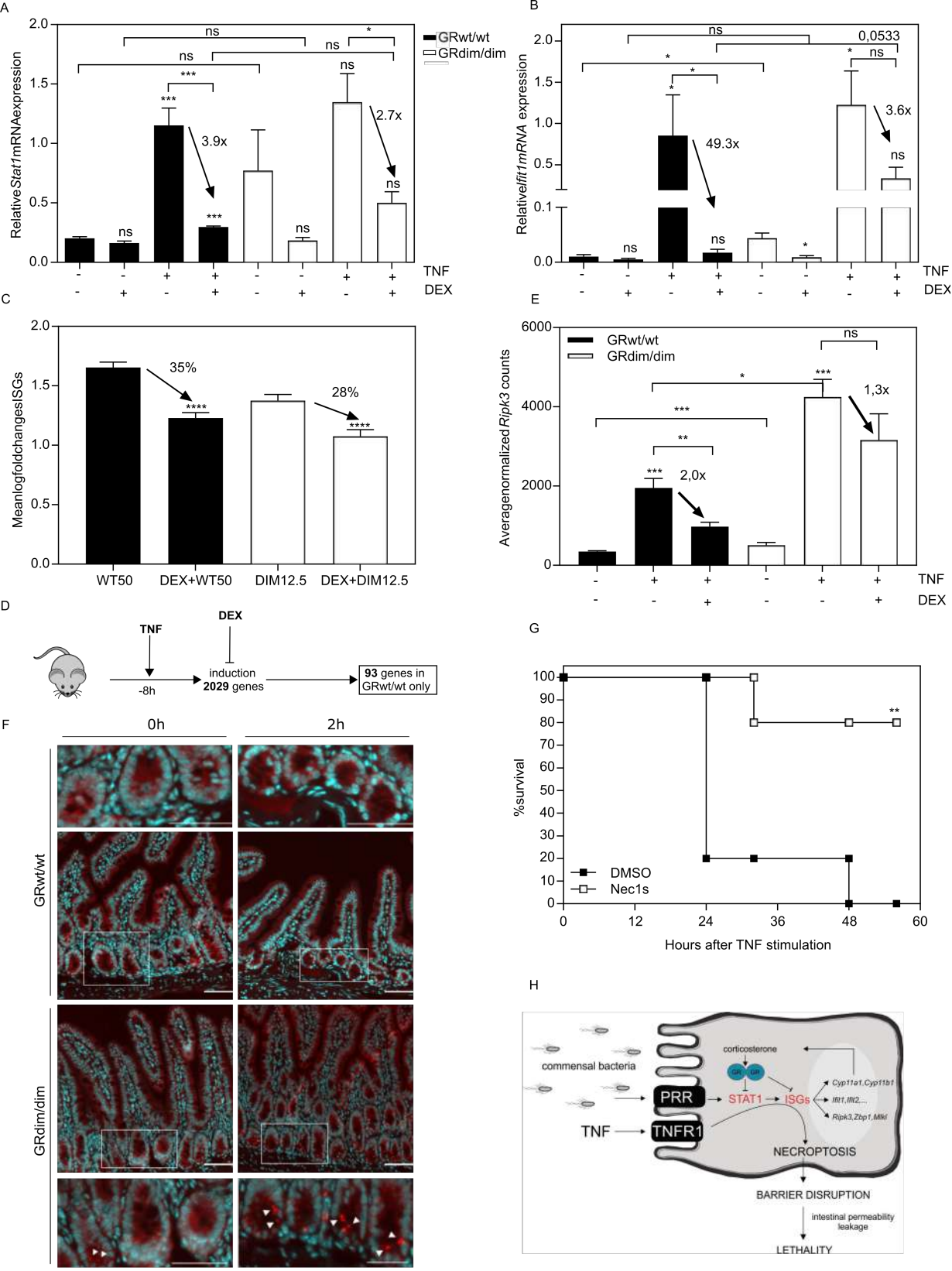

Figure 6: Exogenous GC treatment represses ISGs signature in a GR dimer-dependent way. (A-E) Analysis of the DEX-repression on TNF-induced ISGs based on RNAseq data. GRwt/wt (black) and GRdim/dim (white) mice were pre-treated with vehicle or 10 mg/kg DEX for 30 min followed by challenge with 50 µg or 12.5 µg of TNF respectively (n=3 per group). RNA was isolated and *Stat1* **(A)** and *Ifit1* **(B)** mRNA expression was analyzed via qPCR. **(C)** 736 ISGs were induced by TNF in GRwt/wt and GRdim/dim mice. The impact (Log Fold Change) of DEX pretreatment is depicted as a % reduction. **(D)** In total, across GRwt/wt and GRdim/dim mice, 2029 genes were induced by TNF. 93 genes were only significantly inhibited by DEX in GRwt/wt mice. **(E)** Average normalized counts determined by RNAseq for *Ripk3* which is one of these 93 genes. All bars represent mean ± SEM and statistics were done using two-way ANOVA tests. **(F-G)** GRdim/dim mice have an increased necroptosis signature in IECs. GRwt/wt (black) and GRdim/dim mice (white) were injected with PBS or 12.5 µg TNF (n=5 per group). After 2h, Ripk3 was detected on ileum samples by IHC (**F**; white arrows; representative images are shown). **(G)** GRdim/dim mice were pretreated with vehicle (black) or 250 µg Nec1s (white). 30 min later, mice were challenged with 12.5 µg TNF and survival was monitored (n=5 per group). p- values for survival curves were analyzed with a Logrank test. **** $p < 0.0001$, *** $p < 0.001$, ** $p \leq 0.01$, * $p \leq 0.05$ and ns = not significant. **(H)** General overview of the interaction between the microbiota and local CS production in controlling the ISG signature in IECs. PRR: Patter Recognition Receptor; TNFR: Tumor Necrosis Factor Receptor.